

A Non-Iterative Algorithm for Clearing Two-Layer Energy-Sharing Markets with Voltage Constraints

Tonghua Liu¹, Yifan Su², Member, IEEE, Zhaojian Wang³, Member, IEEE, and Feng Liu^{1,*}, Senior Member, IEEE

¹Department of Electrical Engineering, Tsinghua University, Beijing, China

²School of Electrical Engineering, Chongqing University, Chongqing, China

³School of Automation and Intelligent Sensing, Shanghai Jiao Tong University, Shanghai, China
liuth21@mails.tsinghua.edu.cn, *lfeng@tsinghua.edu.cn

Abstract—Real-time hierarchical energy-sharing markets are promising to coordinate large numbers of prosumers. Still, most existing clearing methods rely on linearized or DC power-flow models and do not explicitly handle reactive power or voltage-security constraints. With AC network constraints, the problem becomes a large-scale bilevel Mathematical Program with Equilibrium Constraints (MPEC) that is difficult to solve in real time. This paper develops a non-iterative clearing algorithm for two-layer energy-sharing markets with voltage constraints. We first derive an efficient best-response function for each lower-layer energy-sharing market and reduce the equilibrium search to one dimension by exploiting the pricing-coupling structure. We then embed this function into the upper-layer network-constrained problem and reformulate the bilevel MPEC as a single-level mixed-integer second-order cone program (MISOCP), which is computationally tractable. Case studies on the IEEE 123-bus system with 12,300 prosumers show that the proposed method preserves nodal voltages within prescribed limits and delivers solutions with maximum errors below 0.01% in 0.829 s.

Index Terms—Energy Sharing; Prosumer; Voltage Security; Non-iterative Algorithm; Hierarchical Market

I. INTRODUCTION

The transition toward carbon neutrality has accelerated the deployment of distributed energy resources (DERs) in distribution networks, transforming end-users from passive consumers into active prosumers [1]–[3]. To coordinate these resources more efficiently, Peer-to-Peer (P2P) energy sharing and local energy markets have emerged as promising mechanisms for enabling direct transactions among prosumers and improving local renewable-energy utilization, economic efficiency, and system flexibility [4]–[6]. Despite this promise, large-scale energy-sharing markets remain difficult to clear in a way that is both computationally scalable and physically feasible.

The main challenge is that market outcomes must respect distribution network constraints, especially voltage security limits, while simultaneously accommodating massive prosumer participation [2], [7]. This challenge becomes particularly acute when nonlinear alternating-current (AC) network constraints are considered, primarily motivating this work.

Existing studies can be cast into three categories. The first category incorporates network constraints directly into local energy markets. Representative approaches combine branch-flow models, second-order cone programming (SOCP) relaxations, Distribution Locational Marginal Pricing (DLMP)-based pricing, and network-aware transactive coordination to mitigate congestion and voltage violations [8]–[13]. While these methods improve physical realism, they are typically

tested on relatively small systems and do not fully address scalability to very large prosumer populations.

The second category focuses on computational scalability. Centralized optimization can, in principle, provide globally optimal clearing results, but it suffers from privacy concerns and severe growth in dimensionality in large-scale settings [14]. Distributed approaches, including game-theoretic methods, decentralized market mechanisms, and Alternating Direction Method of Multipliers (ADMM)-based decompositions, offer several more scalable alternatives [1], [2], [15]. However, once hard physical coupling (e.g. AC power flow) is enforced, especially nodal voltage constraints, iterative distributed algorithms may converge slowly and become difficult to tune in practice [16]–[22].

The third category seeks to combine scalability and physical feasibility through hierarchical or bilevel market architectures [23]–[26]. These frameworks preserve the interaction between local market behavior and network constraints. However, they usually lead to large Mathematical Programs with Equilibrium Constraints (MPECs) that still require extensive iterative computation. Su et al. [27] proposed a highly scalable two-layer market architecture with multiple lower-layer energy-sharing markets (L-ESMs) coordinated by an upper-layer energy-sharing market (U-ESM). This framework, nevertheless, relies on a linearized power-flow model and therefore does not explicitly enforce voltage constraints. Xia et al. [28] moved toward non-iterative market clearing under network constraints. Still, the required power-flow linearization and network reduction may reduce model fidelity in large-scale, heterogeneous distribution networks with a massive number of prosumers.

The aforementioned observations highlight a clear gap in the literature. Existing methods do not simultaneously provide the scalability of a two-layer market architecture with massive prosumers, explicit voltage-security guarantees under AC power flow, and a high-efficiency clearing procedure suitable for real-time implementation. The core bottleneck is that combining massive prosumer participation with nonlinear network constraints yields a high-dimensional bilevel MPEC whose lower-level equilibrium structure is intractable at scale.

To address this challenge and fill this gap, this paper derives an explicit best-response function by unfolding the specific structure of the L-ESM solution, thereby making the lower-layer equilibrium tractable and enabling non-iterative clearing with voltage constraints. The main contributions are

as follows:

- 1) **Efficient algorithms for determining the best-response functions of L-ESMs.** Building upon the established equivalence between the Nash equilibrium in an L-ESM and a convex optimization problem [27], we analyze the solution structure to develop efficient algorithms that determine the best-response function. Unlike standard multi-parametric programming, which requires a high-dimensional active-set search [29], we exploit the L-ESM's specific pricing coupling to collapse the high-dimensional search into a simple 1-dimensional search, thereby remarkably reducing the computational burden. This function serves as a computable surrogate for the complex equilibrium constraints of the L-ESM, eliminating the need for iterative equilibrium search and significantly reducing the computational complexity.
- 2) **A high-efficiency non-iterative market-clearing algorithm with voltage constraints.** By integrating the determined best-response function into the U-ESM and employing a Second-Order Cone Program (SOCP) relaxation of the branch flow model, we transform the original bilevel MPEC into a single-level, tractable Mixed-Integer SOCP (MISOCP). It yields a non-iterative market-clearing algorithm that bridges the critical trade-off between computational efficiency and voltage limits, ensuring network feasibility for large-scale applications.

The rest of the paper is organized as follows. Section II introduces the market model and bilevel formulation. Section III analyzes the L-ESM subproblem. Section IV develops the best-response function and the non-iterative reformulation. Section V reports case studies. Section VI concludes the paper.

II. MARKET DESCRIPTION AND FORMULATION

This work builds on the two-layer hierarchical market architecture proposed by Su et al. [27] and further enforces additional voltage constraints. This architecture naturally decouples the prosumer-level trading details from the network-level operation, thereby providing a tractable framework to enforce rigorous AC power flow and voltage constraints at the upper level. To this end, we replace the original *linearized power flow model* with the *AC branch flow model*, yielding a nonlinear bilevel MPEC with second-order cone constraints, which is challenging to solve.

As shown in Fig. 1, the market comprises a number of prosumers, multiple L-ESMs, and a single U-ESM. The L-ESMs handle local trading among prosumers but do not necessarily achieve a full balance, whereas the U-ESM performs global clearing and enforces network constraints.

Prosumers: Each prosumer is equipped with a load, a non-adjustable power generation device, such as photovoltaic panels, and an adjustable power generation device, such as a gas generator. Prosumers participate in L-ESMs or trade with the electric utility, seeking to minimize their individual costs, which consist of power generation costs and electricity trading fees. The set of prosumers that join L-ESM i is denoted by U_i .

L-ESMs: The L-ESMs, indexed by $i \in \mathcal{N}$, manage the lower-layer trading among a cluster of local prosumers U_i . The

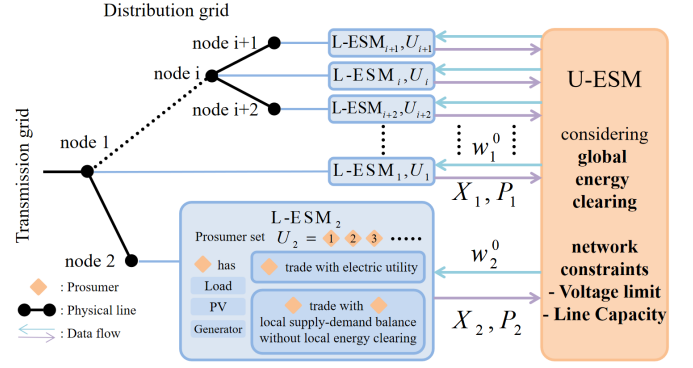


Fig. 1. The two-layer hierarchical market and its clearing scheme

L-ESM adjusts the local energy-sharing price around a base price, relying on the local supply-demand balance. Notably, the L-ESM does not perform a full local clearing; instead, it allows a certain unbalanced portion to spill over to the U-ESM.

U-ESM: The U-ESM coordinates all L-ESMs to enable wider-area energy sharing. Operated as a public utility, it clears the market to minimize the total network loss subject to line limits and voltage constraints. The clearing price is delivered to individual L-ESMs to coordinate their local trading.

The overall trading and market-clearing can be formulated as a Stackelberg game below:

$$w_i^0, P_i, Q_i, P_{ij}, Q_{ij}, l_{ij}, v_i \quad \min \quad \sum_{(i,j) \in \mathcal{E}} r_{ij} l_{ij} \quad (1a)$$

s.t.

$$P_j = \sum_{k:j \rightarrow k} P_{jk} - \sum_{i:i \rightarrow j} (P_{ij} - r_{ij} l_{ij}), \quad \forall j \in \mathcal{N} \quad (1b)$$

$$Q_j = \sum_{k:j \rightarrow k} Q_{jk} - \sum_{i:i \rightarrow j} (Q_{ij} - x_{ij} l_{ij}), \quad \forall j \in \mathcal{N} \quad (1c)$$

$$v_j = v_i - 2(r_{ij} P_{ij} + x_{ij} Q_{ij}) + (r_{ij}^2 + x_{ij}^2) l_{ij}, \quad \forall (i, j) \in \mathcal{E} \quad (1d)$$

$$P_{ij}^2 + Q_{ij}^2 = l_{ij} v_i, \quad \forall (i, j) \in \mathcal{E} \quad (1e)$$

$$\underline{v}_i \leq v_i \leq \bar{v}_i, \quad \forall i \in \mathcal{N} \quad (1f)$$

$$0 \leq l_{ij} \leq \bar{l}_{ij}, \quad \forall (i, j) \in \mathcal{E} \quad (1g)$$

$$\underline{Q}_j \leq Q_j \leq \bar{Q}_j, \quad \forall j \in \mathcal{N} \quad (1h)$$

$$P_j = \sum_{m \in U_j} (x_m^* + p_m^- - p_m^*), \quad \forall j \in \mathcal{N} \quad (1i)$$

$$X_j = \sum_{m \in U_j} x_m^*, \quad \forall j \in \mathcal{N} \quad (1j)$$

$$\sum_{i \in \mathcal{N}} X_i = 0 \quad (1k)$$

$$s_m^* = \{p_m^*, p_m^{+*}, p_m^{-*}, x_m^*\}, \forall m \in U_i, \forall i \in \mathcal{N} \\ = \arg \min_{p_m^+, p_m^-, x_m} \frac{c_m}{2} p_m^2 + b_m p_m + w_i^+ p_m^+ - w_i^- p_m^- - w_i x_m \quad (1l)$$

s.t.

$$D'_m + x_m + p_m^- = p_{solar, m} + p_m + p_m^+, \quad \forall m \in U_i \quad (1m)$$

$$w_i = w_i^0 - a_i X_i, \quad \forall i \in \mathcal{N} \quad (1n)$$

$$0 \leq p_m \leq \bar{p}_m, \quad \forall m \in U_i \quad (1o)$$

$$p_m^+ \geq 0, p_m^- \geq 0, \quad \forall m \in U_i \quad (1p)$$

$$p_m^+ p_m^- = 0, \quad \forall m \in U_i \quad (1q)$$

where \mathcal{E} and \mathcal{N} denote the sets of branches and nodes in the distribution network, respectively; $i, j \in \mathcal{N}$ are the node indices. For a branch $(i, j) \in \mathcal{E}$, r_{ij} and x_{ij} represent the resistance and reactance, while P_{ij} , Q_{ij} , and l_{ij} are the active power flow, reactive power flow, and squared current magnitude, respectively. The symbols \underline{v}_i , \bar{v}_i , and \bar{l}_{ij} represent the lower and upper bounds for voltage magnitude and the upper bound for squared current. At node j , P_j , Q_j , and v_j denote the net injected active power, reactive power, and voltage magnitude. In the upper-layer market, Q_j is modeled as the nodal reactive-power support available to the network operator, with bounds \underline{Q}_j and \bar{Q}_j . For the prosumers, U_i denotes the set of prosumers in L-ESM i . For a specific prosumer $m \in U_i$, x_m is the shared energy (positive for selling, negative for buying); p_m , $p_{solar,m}$, and D'_m denote the adjustable generation, non-adjustable generation, and load, respectively. The parameters $c_m > 0$ and $0 < b_m < w_i^-$ are the cost coefficients of the adjustable generator, which has an upper bound \bar{p}_m . p_m^+ and p_m^- denote the power purchased from and sold to the main grid at prices w_i^+ and w_i^- . The symbol $s_m^* = \{p_m^*, p_m^{+*}, p_m^{-*}, x_m^*\}$ denotes the optimal solution of the sub-problem. Accordingly, the set of optimal solutions for all prosumers in L-ESM i is denoted as $S_i^* = \{s_m^*\}_{m \in U_i}$. Finally, w_i is the local sharing price, w_i^0 is the base price set by the U-ESM, $a_i > 0$ is the price elasticity coefficient regarding the uncleared energy, $P_i := \sum_{m \in U_i} (x_m^* + p_m^{-*} - p_m^{+*})$ denotes the total power exchange with the main grid, and $X_i := \sum_{m \in U_i} x_m^*$ denotes the uncleared sharing energy.

Based on Propositions 1 and 2 in [27], the complementarity constraint (1q) can be relaxed, and the Nash equilibrium of the L-ESM is equivalent to the solution of a convex optimization problem. This equivalence allows us to reformulate the objective function, thereby ensuring that it satisfies the pricing constraint (1n). By further defining the net load as $D_m = D'_m - p_{solar,m}$, the model can be rewritten as follows.

$$\min_{w_i^0, P_i, Q_i, P_{ij}, Q_{ij}, l_{ij}, v_i} \sum_{(i,j) \in \mathcal{E}} r_{ij} l_{ij} \quad (2a)$$

s.t. (1b)–(1k),

$$\begin{aligned} S_i^* &= \{p_m^*, p_m^{+*}, p_m^{-*}, x_m^*\}_{m \in U_i}, \quad \forall i \in \mathcal{N} \\ S_i^* &= \arg \min_{\substack{p_m, p_m^+, p_m^-, x_m \\ \forall m \in U_i}} \left\{ \sum_{m \in U_i} \left(\frac{c_m}{2} p_m^2 + b_m p_m \right. \right. \\ &\quad \left. \left. + w_i^+ p_m^+ - w_i^- p_m^- - w_i^0 x_m \right) + \frac{a_i}{2} \sum_{m \in U_i} x_m^2 \right. \\ &\quad \left. + \frac{a_i}{2} \left(\sum_{m \in U_i} x_m \right)^2 \right\} \quad (2b) \end{aligned}$$

s.t. (1o), (1p),

$$D_m + x_m + p_m^- = p_m + p_m^+, \quad \forall m \in U_i \quad (2c)$$

In this model, the decision variable w_i^0 influences the U-ESM solely through the L-ESM subproblem. To characterize

this influence, we rewrite the L-ESM i subproblem as follows.

$$\begin{aligned} \min_{\substack{p_m, p_m^+, p_m^-, x_m \\ \forall m \in U_i}} \sum_{m \in U_i} \left(\frac{c_m}{2} p_m^2 + b_m p_m + w_i^+ p_m^+ - w_i^- p_m^- \right. \\ \left. - w_i^0 x_m \right) + \frac{a_i}{2} \sum_{m \in U_i} x_m^2 + \frac{a_i}{2} \left(\sum_{m \in U_i} x_m \right)^2 \quad (3) \\ \text{s.t. } D_m + x_m + p_m^- = p_m + p_m^+ : \lambda_{eq,m}, \forall m \in U_i \\ 0 \leq p_m \leq \bar{p}_m : \lambda_{p,lb,m}, \lambda_{p,ub,m}, \forall m \in U_i \\ p_m^+ \geq 0, p_m^- \geq 0 : \lambda_{p,+m}, \lambda_{p,-m}, \forall m \in U_i. \end{aligned}$$

Specifically, w_i^0 affects the U-ESM only through the L-ESM's aggregate variables: the uncleared sharing energy $X_i := \sum_{m \in U_i} x_m^*$ and the total power exchange $P_i := \sum_{m \in U_i} (x_m^* + p_m^{-*} - p_m^{+*})$. If we can explicitly characterize the best-response function $P_i(X_i)$, the implicit L-ESM equilibrium constraints can be replaced by explicit functions, transforming the original bilevel model (2) into the following single-level problem:

$$\min_{X_i, P_i, Q_i, P_{ij}, Q_{ij}, l_{ij}, v_i} \sum_{(i,j) \in \mathcal{E}} r_{ij} l_{ij} \quad (4a)$$

s.t.

$$P_j = \sum_{k:j \rightarrow k} P_{jk} - \sum_{i:i \rightarrow j} (P_{ij} - r_{ij} l_{ij}), \quad \forall j \in \mathcal{N} \quad (4b)$$

$$P_j = P_j(X_j), \quad \forall j \in \mathcal{N} \quad (4c)$$

$$(1c), (1d), (1f), (1g), (1h), (1k)$$

$$P_{ij}^2 + Q_{ij}^2 \leq l_{ij} v_i, \quad \forall (i, j) \in \mathcal{E} \quad (4d)$$

Thus, clearing the market reduces to deriving the best-response function $P_i(X_i)$, which depends on the intrinsic mathematical structure of the subproblem (3).

III. STRUCTURAL PROPERTIES OF THE L-ESM SUBPROBLEM

To derive $P_i(X_i)$, we start with the structural properties of the L-ESM subproblem (3).

Lemma 1. *For the L-ESM subproblem (3), let $(p_m^*, p_m^{+*}, p_m^{-*}, x_m^*)$ be an optimal solution of prosumer m . Then one of the following modes must be satisfied:*

- 1) **Mode 1:** $c_m(x_m^* + D_m) + b_m - w_i^0 + a_i(x_m^* + x_{-m}^*) + a_i x_m^* = 0$ and $p_m^* = x_m^* + D_m$.
- 2) **Mode 2:** $w_i^+ - w_i^0 + a_i(x_m^* + x_{-m}^*) + a_i x_m^* = 0$ and $p_m^* = \min(\bar{p}_m, \frac{w_i^+ - b_m}{c_m})$.
- 3) **Mode 3:** $w_i^- - w_i^0 + a_i(x_m^* + x_{-m}^*) + a_i x_m^* = 0$ and $p_m^* = \min(\bar{p}_m, \frac{w_i^- - b_m}{c_m})$.
- 4) **Mode 4:** $x_m^* = \bar{p}_m - D_m$ and $p_m^* = \bar{p}_m$.

Here, $x_{-m}^* := \sum_{j \in U_i, j \neq m} x_j^*$ for all $m \in U_i$, and $U_{i,k} \subseteq U_i$ denotes the set of prosumers in Mode k ($k = 1, \dots, 4$).

The proof of Lemma 1 is provided in Appendix A.

With the optimal mode of each prosumer identified, we now investigate the functional dependence of the aggregate variables X_i and P_i on the base price w_i^0 .

Although X_i and P_i are formally defined as variables of the U-ESM, their values are entirely determined by the equilibrium solution of the L-ESM subproblem (3) for any given w_i^0 . Therefore, they can be rigorously treated as functions of w_i^0 induced by the L-ESM.

Lemma 2. *For the L-ESM subproblem (3), the aggregate variables $P_i(w_i^0) = \sum_{m \in U_i} (x_m^*(w_i^0) + p_m^-(w_i^0) - p_m^{+*}(w_i^0))$ and $X_i(w_i^0) = \sum_{m \in U_i} x_m^*(w_i^0)$ are piecewise linear in w_i^0 . Furthermore, every breakpoint (i.e., a point where the slope changes) of $P_i(w_i^0)$ is necessarily a breakpoint of $X_i(w_i^0)$.*

Proof. The L-ESM subproblem (3) is a strictly convex quadratic program with linear parameter w_i^0 . Standard results from multi-parametric quadratic programming imply that its optimal solution is a continuous piecewise affine function of w_i^0 [30, Theorem 2, Chapter 1]. Because P_i and X_i are linear combinations of that solution, they are also piecewise linear. Their breakpoints are induced by changes in the active primal or dual constraint set, i.e., by the mode transitions characterized in Lemma 1. \square

Lemma 3. *In the L-ESM subproblem (3), the shared energy of a specific prosumer x_m^* and the uncleared sharing energy of an L-ESM X_i are non-decreasing with respect to the base price w_i^0 . Specifically, within each linear segment where the functions are differentiable:*

$$\frac{dx_m^*}{dw_i^0} \geq 0, \forall m \in U_i; \quad \frac{dX_i}{dw_i^0} \geq 0$$

The equality $\frac{dx_m^*}{dw_i^0} = 0$ holds if and only if prosumer m is operating in Mode 4. The equality $\frac{dX_i}{dw_i^0} = 0$ holds if and only if all prosumers in L-ESM i are in Mode 4.

The proof of Lemma 3 can be found in Appendix B.

Note that when $\frac{dX_i}{dw_i^0} = 0$ (i.e., all prosumers are in Mode 4), P_i remains constant with respect to w_i^0 . This monotonicity ensures P_i is uniquely determined for any given X_i , guaranteeing the well-posedness of the best-response $P_i(X_i)$.

Remark 1. *Standard multi-parametric programming typically relies on enumerating active sets to identify critical regions. However, the specific pricing coupling of the L-ESM guarantees the monotonicity of mode transitions (Lemma 3). This key property degenerates the problem into tracing an ordered sequence of breakpoints along a 1D parameter, enabling direct algorithmic construction without region enumeration.*

IV. BEST-RESPONSE FUNCTION OF L-ESM AND MARKET-CLEARING ALGORITHM

Based on these properties, we develop efficient algorithms to determine the best-response function. We first define auxiliary parameters for each prosumer $m \in U_i$:

$$\alpha_m := \frac{w_i^- - b_m}{c_m} - D_m, \quad (5)$$

$$\beta_m := \frac{w_i^+ - b_m}{c_m} - D_m, \quad (6)$$

$$\gamma_m := \bar{p}_m - D_m. \quad (7)$$

Let $n = |U_i|$. The behavior of $X_i(w_i^0)$ near the lower bound of w_i^0 is first characterized.

Lemma 4. *For the L-ESM subproblem (3), when the base price satisfies $\frac{w_i^0 - w_i^-}{a_i(1+n)} \leq \min\{\min_{m \in U_i}(\alpha_m), \min_{m \in U_i}(\gamma_m)\}$, all prosumers operate in Mode 3, yielding $x_m^* = \frac{w_i^0 - w_i^-}{a_i(1+n)}$ and $X_i = \frac{w_i^0 - w_i^-}{a_i} \frac{n}{1+n}$.*

Proof. According to Lemma 1, under the given condition, all prosumers operate in Mode 3. Summing the corresponding stationarity conditions yields:

$$n(w_i^- - w_i^0) + na_i X_i + a_i X_i = 0. \quad (8)$$

Solving this equation yields the condition for the lemma, and further implies the expression of x_m^* . \square

As the base price w_i^0 increases from the lower bound, prosumers transition between different modes. Recall that $U_{i,k} \subseteq U_i$ denotes the set of prosumers in L-ESM i operating in Mode k (defined in Lemma 1). Such mode transitions introduce breakpoints to the piecewise linear function $X_i(w_i^0)$, as characterized by the following proposition.

Proposition 1. *In the L-ESM subproblem (3), for any prosumer m , the migration path with increasing w_i^0 is determined by the relationship between the parameters $\alpha_m, \beta_m, \gamma_m$:*

- 1) $\gamma_m > \beta_m$: the path is Mode 3 \rightarrow Mode 1 \rightarrow Mode 2.
- 2) $\gamma_m \leq \alpha_m$: the path is Mode 3 \rightarrow Mode 4 \rightarrow Mode 2.
- 3) $\alpha_m < \gamma_m \leq \beta_m$: the path is Mode 3 \rightarrow Mode 1 \rightarrow Mode 4 \rightarrow Mode 2.

Notably, if all prosumers enter Mode 4, X_i becomes constant with respect to w_i^0 and all prosumers remain locked in Mode 4 regardless of further price increases. The specific conditions triggering transitions are:

- 1) $U_{i,3} \rightarrow U_{i,1}$: $p_m^* - D_m = x_m^* = \alpha_m$.
- 2) $U_{i,3} \rightarrow U_{i,4}$: $p_m^* = \bar{p}_m = x_m^* + D_m$ ($x_m^* = \gamma_m$).
- 3) $U_{i,1} \rightarrow U_{i,4}$: $p_m^* = \bar{p}_m = x_m^* + D_m$ ($x_m^* = \gamma_m$).
- 4) $U_{i,1} \rightarrow U_{i,2}$: $p_m^* - D_m = x_m^* = \beta_m$.
- 5) $U_{i,4} \rightarrow U_{i,2}$: $X_i = \frac{w_i^0 - w_i^+}{a_i} - \gamma_m$.

The proof of Proposition 1 can be found in Appendix C.

Based on the piecewise linear structure and the monotonic mode transitions characterized in Proposition 1, the functions $X_i(w_i^0)$ and $P_i(X_i)$ can be efficiently constructed for arbitrary prosumer parameters by iteratively identifying the mode transitions and updating the linear coefficients.

We first present the algorithm for computing $X_i(w_i^0)$. The core idea is to initialize at the lowest price segment where all prosumers operate in Mode 3 and iteratively update their states and linear coefficients as the price increases.

With the piecewise linear function $X_i(w_i^0)$ and the prosumer states determined by Algorithm 1, we now proceed to construct the best-response function $P_i(X_i)$. Algorithm 2 presents the detailed procedure for this derivation.

Model (4) becomes an MISOCP. To ensure tractability, we establish the tightness of its SOCP relaxation.

Assumption 1. *For each node $j \in \mathcal{N}$, the reactive-power support variable Q_j is adjustable within the compact interval $[\underline{Q}_j, \bar{Q}_j]$.*

Algorithm 1: General Computation of $X_i(w_i^0)$

Input: Main grid buying/selling prices w_i^+ , w_i^- ; Price elasticity a_i ; Prosumer parameters $\{c_m, b_m, D_m, \bar{p}_m\}_{m \in U_i}$

Output: Coefficients $\{k'_{X,j}, b'_{X,j}\}$ and breakpoints BP_j for each linear segment

/* Initialization */

Calculate auxiliary parameters $\alpha_m, \beta_m, \gamma_m$ for all $m \in U_i$;

Initialize the state of each prosumer m , denoted as State_m , to Mode 3;

Set segment index $j \leftarrow 0$ and breakpoint $BP_0 \leftarrow -\infty$;

while true do

 /* Step 1: Construct linear segment j */

 Sum the stationarity equations based on current states State_m (Lemma 1) to derive the affine function $X_i = k'_{X,j}w_i^0 + b'_{X,j}$;

 /* Step 2: Determine next breakpoint */

for each prosumer $m \in U_i$ do

 Calculate the candidate trigger price w_m^{next} required to transition from State_m to the next mode based on Proposition 1;

end

$BP_{j+1} \leftarrow \min_m \{w_m^{\text{next}} \mid w_m^{\text{next}} > BP_j\}$;

if $BP_{j+1} = +\infty$ then

 Break the loop;

end

 /* Step 3: Update state */

 Identify the prosumer m^* corresponding to BP_{j+1} and update State_{m^*} to the next mode;

$j \leftarrow j + 1$;

end

return The set of coefficients and breakpoints for all segments

Proposition 2. Under Assumption 1, for the single-level optimization problem (4), the convex relaxation of the branch power flow $P_{ij}^2 + Q_{ij}^2 \leq l_{ij}v_i, \forall (i, j) \in \mathcal{E}$ is tight.

The proof of Proposition 2 can be found in Appendix D.

The overall market-clearing procedure is summarized in Algorithm 3.

V. CASE STUDY

A. Setup

In this section, simulation experiments are conducted using Python and Gurobi on a desktop with an Intel Core i7-14650HX CPU. The IEEE 123-bus distribution feeder is used as the test system, with network parameters adopted from the simplified MATPOWER model in [31]. Each bus is associated with one L-ESM, and each L-ESM contains 100 prosumers, resulting in a total of 12,300 prosumers. The study considers single-period market clearing over a 1-h interval. Under this setting, active power values in kW are numerically equivalent

Algorithm 2: General Computation of $P_i(X_i)$

Input: State sequence $\{\text{State}_m^{(j)}\}$ and coefficients $\{k'_{X,j}, b'_{X,j}\}$ from Algorithm 1; Elasticity coefficient a_i ; Prosumer parameters $\{c_m, b_m, D_m\}_{m \in U_i}$; Auxiliary parameters $\{\alpha_m, \beta_m, \gamma_m\}_{m \in U_i}$

Output: Coefficients $\{k_{P,j}, b_{P,j}\}$ for the piecewise linear function $P_i = k_{P,j}X_i + b_{P,j}$

/* Iterate through each linear segment */

for each segment index j do

 /* Step 1: Obtain inverse coefficients for substitution */

 Initialize $k_{P,j} \leftarrow 0, b_{P,j} \leftarrow 0$;

if $k'_{X,j} \neq 0$ then

$k_{X,j} \leftarrow 1/k'_{X,j}$;

$b_{X,j} \leftarrow -b'_{X,j}/k'_{X,j}$;

else

 Treat segment j as a constant- X_i segment and compute P_i directly from the current prosumer states;

end

 /* Step 2: Calculate $P_i(X_i)$ coefficients */

for each prosumer $m \in U_i$ do

if $\text{State}_m^{(j)} = \text{Mode 1}$ then

$k_{P,j} \leftarrow k_{P,j} + \frac{k_{X,j} - a_i}{c_m + a_i}$;

$b_{P,j} \leftarrow b_{P,j} + \frac{b_{X,j} - b_m - c_m D_m}{c_m + a_i}$;

end

else if $\text{State}_m^{(j)} = \text{Mode 2}$ then

$b_{P,j} \leftarrow b_{P,j} + \min(\beta_m, \gamma_m)$;

end

else if $\text{State}_m^{(j)} = \text{Mode 3}$ then

$b_{P,j} \leftarrow b_{P,j} + \min(\alpha_m, \gamma_m)$;

end

else if $\text{State}_m^{(j)} = \text{Mode 4}$ then

$b_{P,j} \leftarrow b_{P,j} + \gamma_m$;

end

end

end

return $\{k_{P,j}, b_{P,j}\}$

to energy quantities in kWh. Prosumer parameters are synthetically generated, and the same random realization is shared across all compared methods to ensure a fair comparison.

Since renewable energy generation is fluctuating, we manually partition the system into three typical scenarios, as illustrated in Fig. 2:

- **Energy-surplus region:** L-ESMs in this area are set with abundant non-adjustable generation. The net load D for prosumers is randomly selected from $[-40, -20]$ kW.
- **Energy-deficit region:** L-ESMs in this area are set with heavy loads and minimal local generation. The net load D for prosumers is randomly selected from $[20, 40]$ kW.
- **Energy-balance region:** L-ESMs in this area maintain

Algorithm 3: Non-Iterative Clearing for Two-Layer Energy-Sharing Market

Input: Network parameters; L-ESM parameters

$$\{w_i^+, w_i^-, a_i, \{c_m, b_m, D_m, \bar{p}_m\}_{m \in U_i}\}_{i \in \mathcal{N}}$$

Output: Optimal base prices w_i^{0*} , sharing prices w_i^* , uncleared sharing energy X_i^* , and total power exchange P_i^*
for each L-ESM $i \in \mathcal{N}$ do

 Run Algorithm 1 to obtain segments and breakpoints of $X_i(w_i^0)$;

 Run Algorithm 2 to construct the piecewise linear function $P_i(X_i)$;

end

 Formulate the single-level optimization problem (4) using the obtained piecewise linear functions $P_i(X_i)$; Solve the MISOCP to obtain the optimal upper-layer solution, including X_i^* and P_i^* ;

 Determine the operating segment for each L-ESM based on X_i^* and calculate the corresponding base price w_i^{0*} ;

 Calculate the local sharing price $w_i^* = w_i^{0*} - a_i X_i^*$;

/* Verification Step */

for each L-ESM $i \in \mathcal{N}$ do

 Solve the L-ESM subproblem (3) with the obtained w_i^{0*} ;

 Verify that the resulting optimal aggregate variables match X_i^* and P_i^* ;

end
return $w_i^{0*}, w_i^*, X_i^*, P_i^*$

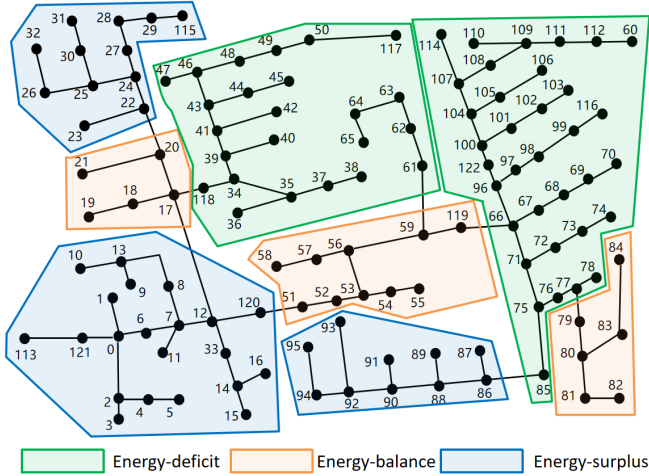
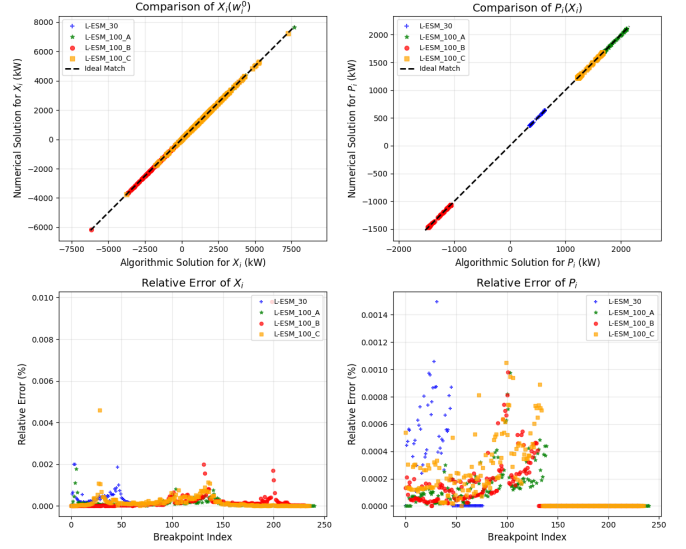


Fig. 2. Configuration of the IEEE 123-bus test system with regional supply-demand scenarios.

 a relative balance. The net load D for prosumers is randomly selected from $[-5, 5]$ kW.

 Following [27], the buying and selling prices w_i^+, w_i^- of the electric utility are set to 0.2\$/kW and 0.05\$/kW, respectively. For each L-ESM, the price elasticity a_i is randomly chosen within the range $[2.5, 5] \times 10^{-3}/|U_i|$ \$/kW. The parameters of prosumers are randomly chosen within the ranges: $c_m \in [0.5, 1] \times 10^{-3}$ \$/kW², $b_m \in [0.01, 0.05]$ \$/kW, and

 Fig. 3. Algorithmic vs. numerical solutions for L-ESMs with varying prosumer counts and parameters. Top: $X_i(w_i^0)$ and $P_i(X_i)$ comparisons. Bottom: Relative errors of X_i and P_i .

 $\bar{p}_m \in [0, 40]$ kW.

B. Validation of Proposed Algorithmic Solution

 To verify the validity of the proposed algorithmic solution, four L-ESMs are tested. The first L-ESM contains 30 prosumers, while the remaining three L-ESMs each consist of 100 prosumers. For the 100-prosumer L-ESMs, the price elasticity coefficients are set to $a = 3 \times 10^{-5}$, $a = 4 \times 10^{-5}$, and $a = 5 \times 10^{-5}$, respectively. Other parameters are randomized as described in Section V.A.

 The comparison involves two solution types: numerical solutions from direct optimization and algorithmic solutions. Specifically, independent variables (w_i^0 or X_i) at each breakpoint of the algorithmic solution are substituted into the optimization problem to evaluate and compare dependent variables (X_i or P_i).

 Fig. 3 shows the results. The top-left and top-right subfigures compare $X_i(w_i^0)$ and $P_i(X_i)$, respectively, with all data points aligning precisely on the diagonal, confirming excellent agreement between algorithmic and numerical solutions. The bottom-left and bottom-right subfigures display relative errors for X_i and P_i , with maximum errors of approximately 0.007% and 0.005%, respectively. Most errors are significantly smaller, validating the high accuracy of the algorithmic solution.

C. Market Clearing Results and Voltage Validation

This subsection presents the market-clearing results for the two-layer energy-sharing market and validates the physical feasibility of the obtained solution, particularly the satisfaction of voltage security constraints.

 Fig. 4 illustrates the spatial distribution of the optimal clearing outcomes across the network. The base prices w_i^0 determined by the U-ESM exhibit clear regional variation. Nodes in the energy-surplus region tend to have higher base prices,

reaching approximately 0.23 \$/kWh, which encourages energy export toward regions with stronger demand. By contrast, nodes in the energy-deficit region exhibit lower base prices, around -0.10 \$/kWh, to encourage energy import. Compared with the base-price profile, the corresponding sharing prices, $w_i = w_i^0 - a_i X_i$, are noticeably smoother across the feeder, suggesting that the local sharing mechanism mitigates regional price disparities while coordinating supply and demand.

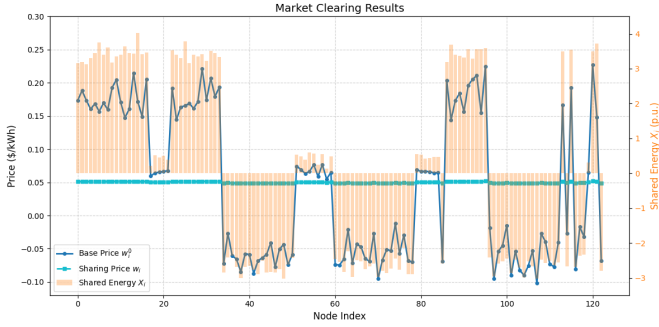


Fig. 4. Spatial distribution of optimal clearing results: (a) base prices w_i^0 , (b) sharing prices w_i , and (c) shared energy X_i .

Physical feasibility requires maintaining node voltages within secure limits. Fig. 5 and Fig. 6 compare the voltage profiles and nodal active/reactive power injection obtained by the proposed method against the benchmark method by Su et al. [27], which employs a linearized power flow model and neglects explicit voltage constraints.

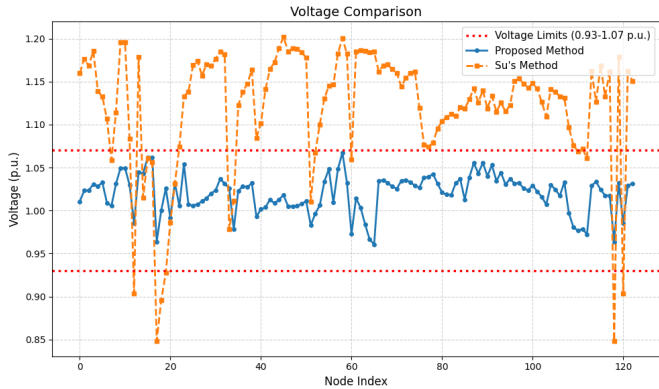


Fig. 5. Comparison of voltage profiles: Proposed method vs. Su's method [27]. The proposed method successfully maintains all voltages within the secure range [0.93, 1.07] p.u. (marked by red dashed lines), while the benchmark method suffers severe overvoltage violations.

The proposed algorithm maintains all node voltages within the secure range (0.93–1.07 p.u.). In contrast, the benchmark method causes severe violations, with voltages exceeding 1.20 p.u. at multiple nodes. These results confirm that rigorous power flow constraints are essential to ensuring the physical feasibility of market-clearing outcomes. The proposed method effectively bridges the gap between market efficiency and physical security by integrating voltage constraints directly into the non-iterative clearing algorithm.

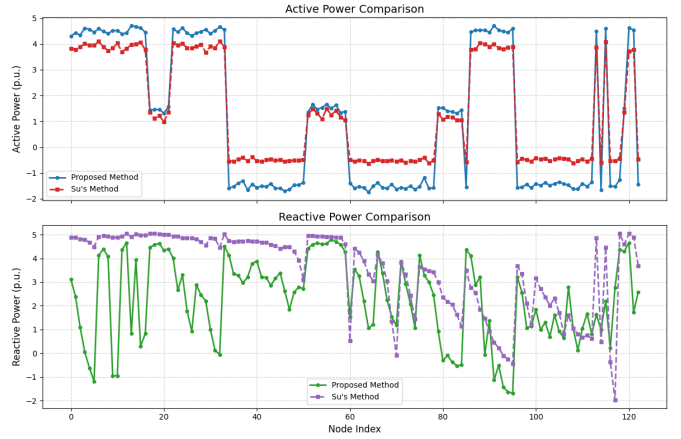


Fig. 6. Comparison of nodal active and reactive power injection profiles.

D. Computation Time Comparison

In this subsection, we compare the computation time of the following four methods:

- 1) **The Proposed Method:** The method introduced in this paper.
- 2) **Su's Method [27]:** A benchmark method that does not consider voltage constraints.
- 3) **The Centralized Method:** An approach that involves solving the entire optimization problem directly.
- 4) **The ADMM Method:** A bilevel iterative method that incorporates both voltage constraints and the individual interests of prosumers.

To ensure a fair comparison reflecting practical implementation, the computation times reported in Table I account for parallel processing where applicable: Su's method considers prosumer-level parallelism; the proposed method considers L-ESM-level parallelism; the ADMM method considers parallel computation of the lower-layer problems; whereas the centralized method cannot be parallelized.

TABLE I
COMPARISON OF COMPUTATION TIMES FOR DIFFERENT NUMBERS OF PROSUMERS.

Prosumer Count	123	369	1,230	6,150	12,300
Proposed Method	0.33ms	0.48ms	1.9ms	0.577s	0.829s
Su's Method	4.03ms	40.6ms	0.12s	0.028s	0.473s
Centralized Method	0.70s	148.06s	$\geq 1h$	-	-
ADMM Method	43.28s	149.02s	$\geq 1h$	-	-

Table I shows that the proposed method scales favorably as the system size increases. The centralized formulation becomes computationally prohibitive once the number of prosumers reaches 10^3 , and the ADMM-based method is likewise hindered by slow convergence under voltage-coupled constraints. Su's method, relying on a linearized power-flow model, remains computationally efficient, but it does not provide explicit voltage-security guarantees. By contrast, the proposed method solves the 12,300-prosumer case in 0.829 s while maintaining all nodal voltages within their limits, supporting its use for large-scale near-real-time market clearing.

E. Social Efficiency

To illustrate the economic necessity of a hierarchical, distributed market for energy sharing, we compare the average costs of prosumers across four market configurations: No Sharing (NS), Local Sharing (LS), Global Sharing (GS), and Global Sharing without Voltage Constraints (GS-NVC).

- 1) **No Sharing (NS):** Prosumers balance independently ($x_m = 0, \forall m \in U_i, \forall i \in \mathcal{N}$).
- 2) **Local Sharing (LS):** Prosumers trade only locally ($X_i = 0, \forall i \in \mathcal{N}$).
- 3) **Global Sharing (GS):** The proposed method.
- 4) **GS without Voltage Constraints (GS-NVC):** The proposed method without enforcing voltage constraints, representing the economic efficiency when physical security is relaxed.

TABLE II
COMPARISON OF COST FOR DIFFERENT ENERGY SHARING SITUATIONS.

Situations	NS	LS	GS	GS-NVC
Cost \$/kWh	0.03551	0.03541	0.03454	0.03452
Total cost \$	6,550.84	6,532.40	6,371.90	6,368.21

Table II shows a monotonic decrease in average cost as the sharing scope expands. Moving from NS to LS yields only a limited reduction, from 0.03551 to 0.03541 \$/kWh, because the restriction $X_i = 0$ confines balancing to individual L-ESMs and does not exploit inter-regional complementarities. The GS configuration reduces the average cost further to 0.03454 \$/kWh by allowing the U-ESM to coordinate energy exchange across the feeder. The GS-NVC case yields a slightly lower cost of 0.03452 \$/kWh but exhibits serious voltage limit violation, which illustrates the expected trade-off between economic performance and network security. Overall, the results suggest that the proposed hierarchical design improves economic efficiency while preserving voltage feasibility.

VI. CONCLUSION

This paper proposes a non-iterative clearing algorithm for the two-layer energy-sharing market with voltage constraints. By deriving the best-response function of the lower-layer market, the original bilevel MPEC is reformulated as a single-level MISOCP that remains tractable for large-scale systems.

Case studies of the IEEE 123-bus system with up to 12,300 prosumers yield three main findings. First, the derived best-response function accurately reproduces the lower-layer equilibrium solution. Second, the proposed method maintains nodal voltages within prescribed limits, unlike benchmark approaches that do not explicitly enforce them. Third, the resulting clearing problem can be solved within sub-second time for the largest test case considered, which suggests strong potential for near-real-time implementation.

The present study is limited to a deterministic, single-period setting and a radial distribution network model. Future work will extend the framework to multi-period coordination with energy storage, uncertainty-aware market clearing, and privacy-preserving implementations.

APPENDIX A PROOF OF LEMMA 1

Proof. Applying the KKT conditions yields the following stationarity conditions:

$$c_m p_m + b_m - \lambda_{\text{eq},m} - \lambda_{p,\text{lb},m} + \lambda_{p,\text{ub},m} = 0 \quad (9a)$$

$$w_i^+ - \lambda_{\text{eq},m} - \lambda_{p,+,m} = 0 \quad (9b)$$

$$-w_i^- + \lambda_{\text{eq},m} - \lambda_{p,-,m} = 0 \quad (9c)$$

$$-w_i^0 + a_i x_m + a_i (x_m + x_{-m}) + \lambda_{\text{eq},m} = 0 \quad (9d)$$

According to Proposition 1 in [27], the optimal solution automatically satisfies the complementarity constraint $p_m^+ p_m^- = 0$. We next analyze the following three mutually exclusive cases for the trading variables p_m^+ and p_m^- :

Case 1: $p_m^+ = 0$ and $p_m^- = 0$. From the power balance constraint, we have $p_m = D_m + x_m$. Substituting $\lambda_{\text{eq},m}$ from (9d) into (9a) and considering the bounds of p_m :

- If $p_m < \overline{p}_m$, then $\lambda_{p,\text{ub},m} = 0$. Rearranging the equations yields the condition for **Mode 1**.
- If $p_m = \overline{p}_m$, it implies the adjustable generator reaches its upper limit, corresponding to **Mode 4**.

Case 2: $p_m^+ > 0$ and $p_m^- = 0$. This implies $\lambda_{p,+,m} = 0$. From (9b), we have $\lambda_{\text{eq},m} = w_i^+$. Substituting this into (9d) yields the condition for **Mode 2**.

Case 3: $p_m^- > 0$ and $p_m^+ = 0$. This implies $\lambda_{p,-,m} = 0$. From (9c), we have $\lambda_{\text{eq},m} = w_i^-$. Substituting this into (9d) yields the condition for **Mode 3**. \square

APPENDIX B PROOF OF LEMMA 3

Proof. By Lemma 2, the optimal solution is piecewise linear in w_i^0 . Therefore, the derivatives exist within each linear segment. We analyze the derivatives on a segment over which the active constraint set remains unchanged.

Based on the modes defined in Lemma 1, we partition the prosumers into three sets for differentiation:

- Ω_1 : Prosumers in Mode 1.
- Ω_{23} : Prosumers in Mode 2 or Mode 3.
- Ω_4 : Prosumers in Mode 4.

This partition reflects the distinct forms of the associated differential equations.

Differentiating the equations satisfied by the prosumer components of the optimal solution in Lemma 1 yields:

Case 1 ($m \in \Omega_1$): $p_m^* = x_m^* + D_m$. From the stationarity condition: $(c_m + a_i) \frac{dx_m^*}{dw_i^0} + a_i \frac{dX_i^*}{dw_i^0} = 1$

Case 2 ($m \in \Omega_{23}$): p_m^+ or p_m^- is active. The stationarity conditions for these modes yield the same differential equation structure: $a_i \frac{dx_m^*}{dw_i^0} + a_i \frac{dX_i^*}{dw_i^0} = 1$

Case 3 ($m \in \Omega_4$): $p_m^* = \overline{p}_m$ and $x_m^* = \overline{p}_m - D_m$. This implies x_m^* is constant: $\frac{dx_m^*}{dw_i^0} = 0$. Denoting $x'_m := \frac{dx_m^*}{dw_i^0}$ and $X'_i := \frac{dX_i^*}{dw_i^0}$, we can rearrange the equations for Ω_1 and Ω_{23} as: $x'_m = \frac{1 - a_i X'_i}{c_m + a_i}$, $\forall m \in \Omega_1$ and $x'_m = \frac{1 - a_i X'_i}{a_i}$, $\forall m \in \Omega_{23}$

Summing the individual derivatives gives the derivative of the aggregate variable $X'_i = \sum_{m \in U_i} x'_m$:

$$\sum_{m \in \Omega_1} \frac{1 - a_i X'_i}{c_m + a_i} + \sum_{m \in \Omega_{23}} \frac{1 - a_i X'_i}{a_i} + \sum_{m \in \Omega_4} 0 = X'_i$$

Rearranging the terms gives the equation for X'_i :

$$\left(1 + \sum_{m \in \Omega_1} \frac{a_i}{c_m + a_i} + |\Omega_{23}|\right) X'_i = \sum_{m \in \Omega_1} \frac{1}{c_m + a_i} + \frac{|\Omega_{23}|}{a_i}$$

We now distinguish the result according to the composition of these sets:

- 1) If $\Omega_1 \cup \Omega_{23} \neq \emptyset$, the right-hand side is strictly positive, and the coefficient on the left-hand side is positive. Thus, $X'_i > 0$.
- 2) If $\Omega_1 \cup \Omega_{23} = \emptyset$ (i.e., all prosumers are in Ω_4), the equation reduces to $X'_i = 0$.

Consequently, $X'_i \geq 0$ always holds. Substituting $X'_i \geq 0$ back into the individual equations:

- For $m \in \Omega_1 \cup \Omega_{23}$: Since $X'_i \leq \frac{1}{a_i}$ (implied by the equation structure), we have $x'_m \geq 0$. Specifically, if $X'_i > 0$, then $x'_m > 0$.
- For $m \in \Omega_4$: $x'_m = 0$ by definition.

This result establishes both the monotonicity and equality conditions, thereby completing the proof. \square

APPENDIX C PROOF OF PROPOSITION 1

Proof. By Lemma 1, the boundaries between modes correspond to specific values of the shared energy x_m^* :

- $U_{i,3} \rightarrow U_{i,1}$ occurs when $x_m^* = \frac{w_i^- - b_m}{c_m} - D_m = \alpha_m$.
- $U_{i,1} \rightarrow U_{i,2}$ occurs when $x_m^* = \frac{w_i^+ - b_m}{c_m} - D_m = \beta_m$.
- Entry into Mode 4 occurs when $x_m^* = \overline{p_m} - D_m = \gamma_m$.

Since x_m^* is non-decreasing with respect to w_i^0 (Lemma 3), the sequence of mode transitions strictly follows the ascending order of the set $\{\alpha_m, \beta_m, \gamma_m\}$:

- 1) If $\gamma_m > \beta_m$, the order is $\alpha_m < \beta_m < \gamma_m$, yielding the path Mode 3 \rightarrow Mode 1 \rightarrow Mode 2.
- 2) If $\gamma_m \leq \alpha_m$, the order is $\gamma_m \leq \alpha_m < \beta_m$, yielding the path Mode 3 \rightarrow Mode 4 \rightarrow Mode 2.
- 3) Otherwise, the order is $\alpha_m < \gamma_m \leq \beta_m$, yielding the path Mode 3 \rightarrow Mode 1 \rightarrow Mode 4 \rightarrow Mode 2.

Finally, consider the locking mechanism. If $U_i = U_{i,4}$, then $X_i = \sum_{m \in U_i} \gamma_m$ is constant. Because the optimal state $x_m^* = \gamma_m$ is enforced by the physical capacity limit $\overline{p_m}$, the partial derivative $\frac{\partial x_m^*}{\partial w_i^0} = 0$. Moreover, the KKT conditions remain satisfied for any w_i^0 large enough to maintain saturation. Hence, all prosumers remain locked in Mode 4. \square

APPENDIX D PROOF OF PROPOSITION 2

Proof. Let $\mathcal{S}^* = \{X_i^*, P_j^*, Q_j^*, P_{ij}^*, Q_{ij}^*, l_{ij}^*, v_i^*\}$ denote an optimal solution set. Given the optimal uncleared energy X_j^* from the lower-level equilibrium, the active power injection

$P_j^* = P_j(X_j^*)$ can be treated as a fixed parameter in the upper-level constraints. Under Assumption 1, tightness is proved by backward induction on the radial network topology.

1. Leaf Branches: Consider a branch $(i, j) \in \mathcal{E}$ where j is a leaf node. At the optimal solution, the power balance equations (1b) and (1c) become $P_{ij}^* = r_{ij} l_{ij}^* - P_j^*$ and $Q_{ij}^* = x_{ij} l_{ij}^* - Q_j^*$. We consider two cases up to the status of voltage constraints.

Case 1: $v_j^* < \overline{v_j}$. Assume for contradiction that the relaxation is not tight, i.e., $l_{ij}^* v_i^* > P_{ij}^{*2} + Q_{ij}^{*2}$. Substituting the optimal values P_{ij}^* and Q_{ij}^* into this inequality yields:

$$l_{ij}^* v_i^* - (r_{ij} l_{ij}^* - P_j^*)^2 - (x_{ij} l_{ij}^* - Q_j^*)^2 > 0. \quad (10)$$

Consider the function $f(l) = l v_i^* - (r_{ij} l - P_j^*)^2 - (x_{ij} l - Q_j^*)^2$. This function is a strictly concave quadratic in l . The feasible region for l_{ij} is the closed interval $\mathcal{L}_{ij} = \{l \mid f(l) \geq 0\}$. Since $f(l_{ij}^*) > 0$, the point l_{ij}^* lies in the interior of \mathcal{L}_{ij} . Therefore, there exists some $l'_{ij} < l_{ij}^*$ such that $f(l'_{ij}) \geq 0$. Because $v_j^* < \overline{v_j}$, l'_{ij} can be chosen sufficiently close to l_{ij}^* so that the voltage constraint $v_j(l'_{ij}) \leq \overline{v_j}$ remains satisfied. This feasible point yields a smaller objective value, which contradicts the optimality of l_{ij}^* . Hence, the constraint must be tight.

Case 2: $v_j^* = \overline{v_j}$. In this scenario, decreasing l_{ij} increases v_j , potentially violating the upper voltage limit. To analyze the trade-off, we express the voltage magnitude v_j as an affine function of the decision variables l_{ij} and Q_j :

$$v_j(l_{ij}, Q_j) = v_i^* - z_{ij} l_{ij} + 2r_{ij} P_j^* + 2x_{ij} Q_j, \quad (11)$$

where $z_{ij} = r_{ij}^2 + x_{ij}^2$. The partial derivatives are: $\frac{\partial v_j}{\partial l_{ij}} = -z_{ij} < 0$, and $\frac{\partial v_j}{\partial Q_j} = 2x_{ij} > 0$, respectively.

Thus, decreasing l_{ij} increases v_j , whereas decreasing Q_j decreases v_j . By Assumption 1, Q_j^* is not located at the lower boundary of its feasible region when $v_j^* = \overline{v_j}$. Therefore, there exists a margin $\bar{\delta} > 0$ such that $Q_j^* - \bar{\delta}$ remains feasible.

We construct a joint perturbation: $l'_{ij} = l_{ij}^* - \epsilon$ and $Q'_j = Q_j^* - \delta$ with $\epsilon, \delta > 0$. To maintain the voltage constraint $v_j(l'_{ij}, Q'_j) = \overline{v_j}$, we use the affine expression above:

$$v_j^* + \frac{\partial v_j}{\partial l_{ij}}(-\epsilon) + \frac{\partial v_j}{\partial Q_j}(-\delta) = \overline{v_j}. \quad (12)$$

Since $v_j^* = \overline{v_j}$, solving for δ yields: $\delta = \frac{z_{ij}}{2x_{ij}} \epsilon$.

Choosing ϵ sufficiently small ensures that $\delta < \bar{\delta}$ and therefore preserves the feasibility of the reactive-power constraint. Define the function $g(\epsilon) = l'_{ij} v_i^* - P_{ij}^{\prime 2} - Q_{ij}^{\prime 2}$, which represents the slack of the SOC constraint under perturbation, where $P'_{ij} = P_{ij}^* - r_{ij} \epsilon$ and $Q'_{ij} = Q_{ij}^* - x_{ij} \epsilon + \delta$. If the SOC constraint were not tight at the optimum, then $g(0) > 0$. By continuity of g , there exists a sufficiently small $\epsilon^* > 0$ such that $g(\epsilon) > 0$ for all $\epsilon \in [0, \epsilon^*]$. Therefore, the perturbed solution $(l_{ij}^* - \epsilon^*, Q_j^* - \frac{z_{ij}}{2x_{ij}} \epsilon^*)$ remains feasible and achieves a smaller objective value, contradicting the optimality of \mathcal{S}^* . Hence, the SOC constraint must be tight.

2. Inductive Step: Assume that for all downstream branches (j, k) , the constraints are tight, implying l_{jk}^* , P_{jk}^* , and Q_{jk}^* are determined constants. Define the aggregate constants:

$$C_P = P_j^* - \sum_{k:j \rightarrow k} P_{jk}^* + \sum_{k:j \rightarrow k} r_{jk} l_{jk}^*, \quad (13)$$

$$C_Q = Q_j^* - \sum_{k:j \rightarrow k} Q_{jk}^* + \sum_{k:j \rightarrow k} x_{jk} l_{jk}^*. \quad (14)$$

The power balance at node j gives: $P_{ij}^* = r_{ij} l_{ij}^* - C_P$ and $Q_{ij}^* = x_{ij} l_{ij}^* - C_Q$. Substituting into the SOC constraint yields a problem that is structurally identical to the leaf-branch case. Repeating the same argument shows that the constraint must also be tight for branch (i, j) .

By induction, the proposition holds for all $(i, j) \in \mathcal{E}$. \square

REFERENCES

- [1] E. A. Soto, L. B. Bosman, E. Wollega, and W. D. Leon-Salas, "Peer-to-peer energy trading: A review of the literature," *Applied Energy*, vol. 283, p. 116268, Feb. 2021. [Online]. Available: <https://linkinghub.elsevier.com/retrieve/pii/S0306261920316585>
- [2] J. Guerrero, A. C. Chapman, and G. Verbic, "Decentralized P2P Energy Trading Under Network Constraints in a Low-Voltage Network," *IEEE Transactions on Smart Grid*, vol. 10, no. 5, pp. 5163–5173, Sep. 2019. [Online]. Available: <https://ieeexplore.ieee.org/document/8513887/>
- [3] Z. Wu, J. Wang, H. Zhong, F. Gao, T. Pu, C.-W. Tan, X. Chen, G. Li, H. Zhao, M. Zhou, and Q. Xia, "Sharing Economy in Local Energy Markets," *Journal of Modern Power Systems and Clean Energy*, vol. 11, no. 3, pp. 714–726, 2023. [Online]. Available: <https://ieeexplore.ieee.org/document/9989335/>
- [4] Y. Chen and C. Zhao, "Review of energy sharing: Business models, mechanisms, and prospects," *IET Renewable Power Generation*, vol. 16, no. 12, pp. 2468–2480, Sep. 2022. [Online]. Available: <https://ietresearch.onlinelibrary.wiley.com/doi/10.1049/rpg2.12438>
- [5] Y. Zhou, J. Wu, C. Long, and W. Ming, "State-of-the-Art Analysis and Perspectives for Peer-to-Peer Energy Trading," *Engineering*, vol. 6, no. 7, pp. 739–753, Jul. 2020. [Online]. Available: <https://linkinghub.elsevier.com/retrieve/pii/S2095809920301405>
- [6] M. Zedan, M. Nour, G. Shabib, L. Nasrat, and A.-A. Ali, "Review of peer-to-peer energy trading: Advances and challenges," *e-Prime - Advances in Electrical Engineering, Electronics and Energy*, vol. 10, p. 100778, Dec. 2024. [Online]. Available: <https://linkinghub.elsevier.com/retrieve/pii/S2772671124003589>
- [7] T. Kleinjan and J. Yang, "Voltage Support Based Peer-to-Peer Energy Trading Scheme with Reactive Power Compensation," in *2022 IEEE PES Innovative Smart Grid Technologies Conference Europe (ISGT-Europe)*. Novi Sad, Serbia: IEEE, Oct. 2022, pp. 1–5.
- [8] M. Farivar and S. H. Low, "Branch Flow Model: Relaxations and Convexification—Part I," *IEEE Transactions on Power Systems*, vol. 28, no. 3, pp. 2554–2564, Aug. 2013. [Online]. Available: <http://ieeexplore.ieee.org/document/6507355/>
- [9] M. Z. Golombahri, M. Shakarami, and M. Doostizadeh, "Decentralized Energy and Flexibility Markets for Integrated Electricity and Heat Networks: Optimal Allocation, Trading, and Leasing," *IET Generation, Transmission & Distribution*, vol. 19, no. 1, p. e70195, Jan. 2025. [Online]. Available: <https://ietresearch.onlinelibrary.wiley.com/doi/10.1049/gtd2.70195>
- [10] Y. Wu, J. Shi, G. J. Lim, L. Fan, and A. Molavi, "Optimal Management of Transactive Distribution Electricity Markets With Co-Optimized Bidirectional Energy and Ancillary Service Exchanges," *IEEE Transactions on Smart Grid*, vol. 11, no. 6, pp. 4650–4661, Nov. 2020.
- [11] X. Yan, M. Song, J. Cao, C. Gao, X. Jing, S. Xia, and M. Ban, "Peer-to-Peer transactive energy trading of multiple microgrids considering renewable energy uncertainty," *International Journal of Electrical Power & Energy Systems*, vol. 152, p. 109235, Oct. 2023. [Online]. Available: <https://linkinghub.elsevier.com/retrieve/pii/S0142061523002922>
- [12] M. Yan, M. Shahidehpour, A. Paaso, L. Zhang, A. Alabdulwahab, and A. Abusorrah, "Distribution Network-Constrained Optimization of Peer-to-Peer Transactive Energy Trading Among Multi-Microgrids," *IEEE Transactions on Smart Grid*, vol. 12, no. 2, pp. 1033–1047, Mar. 2021. [Online]. Available: <https://ieeexplore.ieee.org/document/9235517/>
- [13] D. Yan and Y. Chen, "Distributed Coordination of Charging Stations With Shared Energy Storage in a Distribution Network," *IEEE Transactions on Smart Grid*, vol. 14, no. 6, pp. 4666–4682, Nov. 2023.
- [14] Udabala, Y. Li, J. Liu, Y. Li, Y. Gong, and Z. Xu, "Aggregated Energy Interaction and Marketing for the Demand Side with Hybrid Energy Storage Units," *Journal of Electrical Engineering & Technology*, vol. 20, no. 1, pp. 169–184, Jan. 2025. [Online]. Available: <https://link.springer.com/10.1007/s42835-024-02017-0>
- [15] N. Yaagoubi and H. T. Mouftah, "Energy Trading in the Smart Grid: A Distributed Game-Theoretic Approach," *Canadian Journal of Electrical and Computer Engineering*, vol. 40, no. 2, pp. 57–65, 2017. [Online]. Available: <https://ieeexplore.ieee.org/document/7999299/>
- [16] N. S. M. Noorpi, E. Aprilia, W. Zhang, and K. Meng, "ADMM-based Optimum Power Flow in Nested Microgrids," in *2020 International Conference on Smart Grids and Energy Systems (SGES)*. Perth, Australia: IEEE, Nov. 2020, pp. 916–921. [Online]. Available: <https://ieeexplore.ieee.org/document/9364407/>
- [17] H. Lou and S. Fujimura, "ADMM -Based Distributed Algorithm for Energy Management in Multi-Microgrid System," *IEEJ Transactions on Electrical and Electronic Engineering*, vol. 19, no. 1, pp. 79–89, Jan. 2024.
- [18] S. Baek, S. Hamm, Y.-J. Kim, and J. P. S. Catalão, "Security-Constrained P2P Energy Trading Strategy via Priced-Based Regularization of ADMM in a Distribution Network," *IEEE Access*, vol. 12, pp. 152972–152988, 2024. [Online]. Available: <https://ieeexplore.ieee.org/document/10720016/>
- [19] W. Deng, M.-J. Lai, Z. Peng, and W. Yin, "Parallel Multi-Block ADMM with $\mathcal{O}(1/k)$ Convergence," *Journal of Scientific Computing*, vol. 71, no. 2, pp. 712–736, May 2017. [Online]. Available: <http://link.springer.com/10.1007/s10915-016-0318-2>
- [20] H. J. Liu, W. Shi, and H. Zhu, "Distributed Voltage Control in Distribution Networks: Online and Robust Implementations," *IEEE Transactions on Smart Grid*, vol. 9, no. 6, pp. 6106–6117, Nov. 2018.
- [21] C. Feng, B. Liang, Z. Li, W. Liu, and F. Wen, "Peer-to-Peer Energy Trading Under Network Constraints Based on Generalized Fast Dual Ascent," *IEEE Transactions on Smart Grid*, vol. 14, no. 2, pp. 1441–1453, Mar. 2023. [Online]. Available: <https://ieeexplore.ieee.org/document/9744103/>
- [22] L. Dong, S. Zhang, T. Zhang, Z. Wang, J. Qiao, and T. Pu, "DSO-prosumers dual-layer game optimization based on risk price guidance in a P2P energy market environment," *Applied Energy*, vol. 361, p. 122893, May 2024. [Online]. Available: <https://linkinghub.elsevier.com/retrieve/pii/S0306261924002769>
- [23] Y. Lin and J. Wang, "Nested Bilevel Energy Hub Bidding and Pricing With Price-Responsive Demand," *IEEE Transactions on Smart Grid*, vol. 14, no. 2, pp. 1418–1429, Mar. 2023. [Online]. Available: <https://ieeexplore.ieee.org/document/9776509/>
- [24] Q. Hong, F. Meng, J. Liu, and R. Bo, "A bilevel game-theoretic decision-making framework for strategic retailers in both local and wholesale electricity markets," *Applied Energy*, vol. 330, p. 120311, Jan. 2023. [Online]. Available: <https://linkinghub.elsevier.com/retrieve/pii/S0306261922015689>
- [25] A. K. Zarabie, S. Das, and M. N. Faqiry, "Fairness-Regularized DLMP-Based Bilevel Transactive Energy Mechanism in Distribution Systems," *IEEE Transactions on Smart Grid*, vol. 10, no. 6, pp. 6029–6040, Nov. 2019. [Online]. Available: <https://ieeexplore.ieee.org/document/8626512/>
- [26] N. Noorfatima, J. Jung, A. Onen, and Y. Yoldas, "Bilevel Peer-to-Peer Energy Trading to Maintain Network Quality and Benefit Distribution," *IEEE Transactions on Applied Superconductivity*, vol. 34, no. 8, pp. 1–5, Nov. 2024.
- [27] Y. Su, P. Yang, K. Kang, Z. Wang, N. Qi, T. Liu, and F. Liu, "Sharing energy in wider area: A two-layer energy sharing scheme for massive prosumers," *Applied Energy*, vol. 392, p. 125968, Aug. 2025. [Online]. Available: <https://linkinghub.elsevier.com/retrieve/pii/S0306261925006981>
- [28] Y. Xia, Q. Xu, J. Fang, and F. Li, "Non-Iterative Decentralized Peer-to-Peer Market Clearing in Multi-Microgrid Systems via Model Substitution and Network Reduction," *IEEE Transactions on Power Systems*, vol. 39, no. 2, pp. 2922–2935, Mar. 2024.
- [29] A. Gupta, S. Bhartiya, and P. Nataraj, "A novel approach to multiparametric quadratic programming," *Automatica*, vol. 47, no. 9, pp. 2112–2117, Sep. 2011.
- [30] E. N. Pistikopoulos, Ed., *Multi-parametric programming: theory, algorithms and applications*, ser. Process systems engineering. Weinheim: Wiley-VCH, 2007, no. 1.
- [31] L. Bobo, A. Venzke, and S. Chatzivasileiadis, "Second-Order Cone Relaxations of the Optimal Power Flow for Active Distribution Grids," Jun. 2020.